



1 **Machine learning based streamflow prediction in a hilly catchment for future scenarios**
2 **using CMIP6 data**

3 Dharmaveer Singh^{1*}, Manu Vardhan², Rakesh Sahu³, Debrupa Chatterjee¹, Pankaj Chauhan⁴,
4 and Shiyin Liu^{5*}

5
6 1. Symbiosis Institute of Geo-informatics, Symbiosis International (Deemed University),
7 Pune-411004 (India).

8 2. Computer Science and Engineering Department, National Institute of Technology Raipur,
9 Raipur-492010 (India)

10 3. Department of Civil Engineering, Indian Institute of Technology Bombay, Mumbai-
11 400076 (India)

12 4. Wadia Institute of Himalayan Geology, Dehradun-248001 (India)

13 5. Institute of International Rivers and Eco-security, Yunnan University, Kunming - 650091
14 (China)

15

16 *Corresponding author's email: veermnit@gmail.com and shiyin.liu@ynu.edu.cn

17

18



19 **Abstract**

20 The alteration in river flow patterns, particularly those that originate in the Himalayas, has
21 been caused by the increased temperature and rainfall variability brought on by climate
22 change. Due to the impending intensification of extreme climate events, as predicted by the
23 Intergovernmental Panel on Climate Change (IPCC) in its sixth assessment report, it is more
24 essential than ever to predict changes in streamflow for future periods. Despite the fact that
25 some research has utilised machine learning-based models to predict streamflow patterns in
26 response to climate change, very few studies have been undertaken for a mountainous
27 catchment, with the number of studies for the western Himalaya being so small as to be
28 considered insignificant. This study investigates the capability of different machine learning
29 (ML) models, including the Gaussian Linear Regression Model (GLM), Gaussian
30 Generalized Additive Model (GAM), Multivariate Adaptive Regression Splines (MARS),
31 Artificial Neural Network (ANN), and Random Forest (RF), in streamflow prediction over
32 the Sutlej River Basin in western Himalaya during the periods 2041-2070 (2050s) and 2071-
33 2100 (2080s) for two greenhouse gas trajectories (SSP245 and SSP585). Coupled Model
34 Intercomparison Project Phase 6 (CMIP6) bias corrected data downscaled at grid resolution
35 of $0.25^{\circ} \times 0.25^{\circ}$ for 6 General Circulation Models (GCMs) were used for this purpose. Four
36 different rainfall scenarios (R_0 , R_1 , R_2 , and R_3) were applied to the models trained with daily
37 data (1979-2009) at Kasol (the outlet of the basin) in order to better understand how
38 catchment size and the geo-hydro-morphological aspects of the basin affect runoff. RF model
39 with rainfall scenario R_3 which outperformed other models during the training and testing
40 period therefore was chosen to simulate streamflow in the Sutlej River in the 2050s and
41 2080s under the SSP245 and SSP585 scenarios. The mean ensemble of model results show
42 that the mean annual streamflow of the Sutlej River is expected to rise between 2050s and
43 2080s by 5.51 to 6.04% for SSP585 and by 6.65 to 6.75% for SSP245. The seasonal



44 streamflow also is expected to increase in the 2050s and 2080s under both emission
45 scenarios, with the exception of the pre-monsoon, where a decline in streamflow is
46 anticipated for SSP585 in the 2080s. However, under both the emission scenarios, there
47 seemed to be significant variation in the streamflow simulations among the individual models
48 for various time periods. It has been found that the pattern of this variability is highly
49 correlated with the pattern of precipitation and temperature predicted by various GCMs for
50 future emission scenarios. The present study will therefore assist in strategy planning for
51 ensuring the sustainable use of water resources downstream by acquiring a knowledge of the
52 nature and causes of unpredictable streamflow patterns.

53 **Keywords:** Machine learning models; streamflow; climate change; CMIP6; western
54 Himalaya

55



56 **1. Introduction**

57 Human-induced global warming has altered patterns of the rainfall worldwide (Goswami et
58 al., 2006; Trenberth, 2011), and also increased risks of extreme events such as the droughts
59 and floods (Easterling et al., 2000; Trenberth et al., 2015; Otto et al., 2017). It has impacted
60 hydrology of many river basins globally, including variation in streamflow (Gerten et al.,
61 2008; Lutz et al., 2014; Nepal and Shrestha, 2015; Singh et al. 2015a; Ali et al., 2018; Singh
62 et al., 2022). A study of long-term (1948-2004) streamflow (discharge) data of 200 largest
63 rivers of the globe showed considerable change in their annual discharge, however, results
64 were statistically significant only for 64 rivers. Out of which 45 were marked with decreasing
65 trends and the remaining 19 showed increasing trends in their annual discharge (Dai et al.,
66 2009). Similar trends in discharge of the rivers were reported also at regional scale: Asia
67 (Kundzewicz et al., 2009; Krysanova et al., 2015), Europe (Stahl et al., 2010; Stahl and
68 Tallaksen, 2012) and America (Pasquini and Depetris, 2007). Moreover, it has been
69 established that the effects of rainfall variation and extreme events on annual discharge are
70 likely strong compared with other drivers (Miller et al., 2012; Van der Wiel et al., 2019). A
71 projected rise of $\sim 2^{\circ}\text{C}$ to 5°C in mean annual global temperature by 2100 under higher
72 greenhouse gas emission scenarios as predicted from the General Circulation Models
73 (GCMs) (Gao et al., 2017) will considerably affect the rainfall pattern (intensity and amount)
74 and may have adverse effects on hydrological cycles (Okai and Kanae 2006; Haddeland et
75 al., 2014). This would subsequently impact availability of water resources and present
76 challenges for their management since a rise in the demand of water is also predicted (Lutz et
77 al., 2019). Therefore, it is indispensable to know the underlying hydrological dynamics
78 occurring within a basin in context of climate change for effective management and
79 sustainable use of the water resources.



80 The underlying hydrological processes controlling rainfall-runoff generation in a basin can be
81 understood with the use of a hydrological model which is based on complex mathematical
82 equations and theoretical laws governing physical processes in the basin (Kirchner, 2006;
83 Singh et al., 2019). It simulates/or predicts response of the basin to climatological forcings
84 such as the rainfall (Sood and Smakhtin, 2009) and generate synthetic time series of
85 hydrological data that could be used by water managers and scientists for varied applications
86 ranging from water budgeting and partitioning (Conan et al., 2003; Schreiner-McGraw and
87 Ajami, 2020; Masse-Dufresne et al., 2021) to inundation mapping and modelling (Mahto et
88 al., 2022). A hydrological model is supposed not only to have a good predictive power but
89 also the ability of capturing relationships among the forcing factors and catchment response
90 so that an accurate estimate of rainfall-runoff could be made (Shortridge et al., 2016).
91 However, until now, there is no hydrological model that can simulate basin-behaviour
92 universally well against all the hydrological challenges inflicted from climate change and
93 human-interventions (Yang et al., 2019). As a result, many hydrological models have been
94 devised considering functioning and robustness of models in explaining underlying
95 complexity in quantifying basin-scale response to small-scale spatial complexity of physical
96 processes (Shortridge et al., 2016; Herath et al., 2021). Broadly, these can be grouped into
97 two categories: physical or process-based models and empirical or data-driven models (Yang
98 et al., 2019; Kabir et al., 2020). The latter category of models uses a mathematical
99 relationship established between runoff and affecting factors in the basin for deriving the
100 runoff (Muhammad Adnan, 2019).

101

102 It is purported that the data-driven model despite of inherited limitations over physical
103 interpretability of processes has outperformed the physical models in terms of prediction
104 accuracy in many hydrological applications (Shortridge et al., 2016; Muhammad Adnan,



105 2019; Kabir et al., 2020; Herath et al., 2021). Also, they are preferred over the physical
106 models for rainfall-runoff modelling/or streamflow prediction modelling due to limited
107 requirements of data as inputs, where data limitation is the major challenge (Beven, 2011).
108 These models in past were heavily criticised on the ground of being incompetent to model the
109 non-linear behaviour of streamflow (Yang et al., 2019). But recent developments in
110 computational intelligence, in the area of Machine Learning (ML) in particular, have greatly
111 expanded the capabilities of empirical modelling. This resulted in the development of many
112 non-linear models such as the Artificial Neural Network (ANN), Random Forest (RF), and
113 Support Vector Machine (SVM), which can capture and model non-stationarity of the
114 rainfall-runoff relationships (Shortridge et al., 2016; Muhammad Adnan, 2019; Yang et al.,
115 2019). Despite of the significance potentials of the ML models in streamflow prediction,
116 relevant studies assessing the application of these models for streamflow prediction under
117 future scenarios over the mountainous basins are limited due to non-availability of long-term
118 data. Hence, it is important to test whether machine learning approaches can be effectively
119 used over a mountainous river basin to predict streamflow using hydro-meteorological
120 variables and CMIP6 scenarios as the input data.

121

122 With a catchment area of 56874km² (up to Bhakara Dam), the Sutlej also pronounced as
123 ‘Satluj’ is an important river in the western Himalayas and runs through diverse climatic
124 zones. The flow in the upper and middle catchment is primarily impacted by glacier/snow
125 melt induced by seasonal temperature shift and preceding winter precipitation, while the
126 lower section of the catchment area is mostly regulated by rainfall both in the winter and
127 during the monsoon season (Singh and Jain, 2002; Archer, 2003; Miller et al., 2012). Based
128 on data from the period 1986–1996, Singh and Jain (2002) estimated the mean yearly
129 contribution of snow/glacier melt and rainfall to the Sutlej River as being 59% and 41%,



130 respectively. However, the discharge in the river peaks is directly related to the peak in
131 rainfall during the monsoon (Lutz et al., 2014). Recent studies on this basin has raised
132 concerns about the implications of climatic changes on streamflow since a warming climate
133 has brought changes in the amount and spatial-temporal distribution of precipitation (Singh et
134 al., 2014; Singh et al., 2015b). Previous research has only used process-based hydrological
135 models to date when examining the effects of climate change (past and present) on
136 streamflow patterns in the region (Singh and Jain, 2002; Singh et al., 2015a; Ali et al., 2018;
137 Shukla et al., 2022), which leaves a gap in the use of machine learning models. This study
138 very first time examines the potential of various ML models namely, Gaussian Linear
139 Regression Model (GLM), Gaussian Generalized Additive Model (GAM), Multivariate
140 Adaptive Regression Splines (MARS), ANN and RF in streamflow prediction over the Sutlej
141 River Basin (rainfall dominated zone) in western Himalaya during the period 2041-2070
142 (2050s) and 2071-2100 (2080s) and its relationship to climate variability.

143

144 **2. Study Area**

145 Sutlej is a Trans Himalayan river with its origin in the Rakshastal Lake (elevation:4570m)
146 near to the Mansarovar Lake in the western Himalaya. It is the largest tributary of the Indus
147 River. The total catchment area of the Sutlej River upto Bhakara Dam is about 56874km², of
148 which 22305 km² (extending between Spiti Valley and Bhakara) falls within India. It is a high
149 relief catchment (elevation: 350-6558 m) dominated by rainfall, but also received significant
150 contribution from glacier/snow melt. The selected study area is a sub-catchment within the
151 basin (Figure 1), with an area of 2457 km². It is dominated mostly by forests (56.20%),
152 grassland (26.4%), agricultural lands (17.1%), and glaciers and snow covers (0.3%) (Singh et
153 al., 2015a). The details of the sub-catchment are summarised in Table 1.

154

Figure 1: The location of the sub-catchment within Sutlej River Basin



155

156 The basin bestowed with the hydropower potential of about 9226.75MW is climatologically
157 sensitive and, at present, facing the challenges created due to climate change and human's
158 interventions (Singh et al., 2015b and 2015c). Change in future climate will alter patterns of
159 flow in river and further could affect water resources and hydroelectric power production
160 (Singh et al., 2014). Therefore, the present study will provide useful insight to devise better
161 strategy for the management of water resources in the Sutlej basin.

162 Table 1: Characteristics of the study catchment over the evaluation period of 1979–2009

163

164 **3. Description of the Data and Methods**

165 The methodology involved in predicting streamflow for the period 2021-2100 in the Sutlej
166 River include: 3.1) collection of hydro-meteorological data, 3.2) selection of machine
167 learning models, and 3.3) performance evaluation of the developed models. These are
168 described in details under following sub-headings:

169

170 **3.1 Hydro-meteorological data**

171 The daily rainfall, temperature (T_{\max} and T_{\min}), relative humidity, solar radiation, wind speed
172 and discharge data used to study performance of the different machine learning models on
173 streamflow modelling were collected for 31 years i.e. 1979-2009. Rainfall, temperature and
174 discharge data were obtained from the Bhakara Beas Management Board (BBMB), while
175 relative humidity, solar radiation and wind data were extracted from the Global Weather Data
176 (<http://globalweather.tamu.edu/>). The outputs from the CMIP6, the latest generation of
177 climate models, were used for streamflow prediction. Even by using downscaled GCMs,
178 however, regional climate change projections inherit biases from the GCM boundary
179 conditions, which were corrected in the dataset detailed in Mishra et al. (2020) for South



180 Asia. This dataset provides bias-corrected downscaled climate change projections for 13
181 CMIP6 models and four GHG emission scenarios (SSP126, SSP245, SSP370, and SSP585),
182 the latter are briefly summarised in Riahi et al. (2017). The data are available at a daily time-
183 scale and horizontal spatial resolution of $0.25^{\circ} \times 0.25^{\circ}$. This study used the bias-corrected
184 downscaled regional climate change scenarios from six CMIP6 GCMs: 1) Beijing Climate
185 Centre Climate System Model version 2 (BCC-CSM2-MR), 2) Russian Institute for
186 Numerical Mathematics Climate Model Version 4.8 (INM-CM4-8), 3) Russian Institute for
187 Numerical Mathematics Climate Model Version 5.0 (INM-CM5-0), 4) Australian Community
188 Climate and Earth System Simulator-Earth System Model version 1 (ACCESS- ESM1.5), 5)
189 Australian Community Climate and Earth System Simulator-coupled model version 2
190 (ACCESS-CM2), and 6) Earth Consortium-Earth 3 Veg Model (EC-Earth-veg) which were
191 selected based on their performances in simulating precipitation and temperature over the
192 western Himalaya to examine future patterns in streamflow for the period 2021-2100 in the
193 Sutlej River according to two GHG emissions scenarios: SSP245 and SSP585.

194

195 **3.2 Selection of machine learning models for streamflow modelling**

196 In this study, five machine learning models namely GLM, GAM, MARS, ANN and RF were
197 selected and their performances in predicting streamflow in Sutlej River were compared.
198 These are regression based models which capture relationship between the predictors
199 (dependent variables) and predictand (independent variables) and provide value of the output
200 variables (Muhammad Adnan, 2019; Kabir et al., 2020). The models were trained with daily
201 data recorded during 1979-2009 at Kasol (the gauging site), the outlet of the basin. However,
202 prior to building the models, all of the data were normalized using standard normalization
203 techniques to get features on a common scale. Further, the entire data set was split into
204 training and testing datasets since a cross-validation method was adopted in this study. The



205 training dataset (80%) was used for fitting the models whereas testing dataset was used for
206 checking model accuracy (20%). Under the cross-validation method, the process was
207 repeated until every part of the allocated data was used in testing (Kabir et al., 2020). This
208 technique enables the buildout of generalising models, that if tested correct could be applied
209 in predicting flow for ungauged watersheds of similar geographical and climatic
210 characteristics where past rainfall/runoff are not available.

211

212 Five different program codes were written in python language for GLM, GAM, MARS, ANN
213 and RF simulations. Out of these five selected models, GLM, GAM and MARS are linear
214 models whereas other two i.e. ANN and RF are non-linear in nature (Shortridge et al., 2016;
215 Yang et al., 2019; Herath et al., 2021). Additionally, excluding GLM all of the remaining ML
216 models are based on non-parametric regression approach where functional relationship
217 between predictor and predictand are not predetermined but can be adjusted to capture
218 unusual or unexpected features of the data (Shortridge et al., 2016). A detailed description of
219 these models can be found elsewhere (Shortridge et al., 2016; Muhammad Adnan, 2019;
220 Yang et al., 2019; Kabir et al., 2020; Herath et al., 2021). Six variables namely rainfall, T_{\max} ,
221 T_{\min} , relative humidity, solar radiation and wind speed were used as the inputs for developing
222 the models. Additionally, these models were simulated under four rainfall scenarios: rainfall
223 on the same day (R_0), rainfall lagged by one day (R_1) and rainfall lagged by two days (R_2)
224 and rainfall lagged by three days (R_3) to understand control of catchment size and geo-hydro-
225 morphological characteristics of the basin in generating runoff. While, remaining
226 meteorological parameters were held constant during the processes.

227

228 **3.3 Model performance evaluation**



229 It has been found that overfitting in a model may lead to large errors in out-of-sample
230 predictions (Hastie et al., 2009). Therefore, it has been evaded by establishing model
231 parameters for GLM, GAM, MARS, ANN and RF through automated hyperparameter tuning
232 methods. 500 bootstrap resamples of the training data set were generated for each parameter
233 value to be assessed. Table 2 presents the information on the specific parameters evaluated
234 for each model.

235 Table 2: The information on hyper parameters used for estimating model parameters

236

237 Three evaluation criteria were used to assess the daily streamflow predictions of different
238 models. These were coefficient of determination (R^2), ratio of the root mean square error to
239 the standard deviation of measured data (RSR) and mean absolute error (MAE). The RSR
240 and MAE are calculated as given in equation 4 and 5, respectively.

241

$$RSR = \frac{\sqrt{\sum_{i=1}^n \frac{(P_i - O_i)^2}{n}}}{STDEV_{Obs}} \dots\dots\dots(1)$$

242

243

$$MAE = \frac{\sum_{i=1}^n |P_i - O_i|}{n} \dots\dots\dots(2)$$

244

245

246 where P_i are the predicted values and O_i are the observed values, n accounts for the number
247 of samples, \bar{O} represents the mean of observed data, and \bar{P}_i is the mean of predicted data and
248 $STDEV_{Obs}$ refers to the standard deviation of observed values. R^2 explains the correlation
249 between observed and predicted values, lies between 0 and 1. R^2 values between 0.6 to 0.7
250 are considered satisfactory, 0.85 to 1 are very good and below 0.4 are unsatisfactory. The
251 lower is the RSR value, the better is the model. Values greater than 0.7 are unsatisfactory



252 whereas those lying between 0 and 0.5 come in the very good range. Mean absolute error
253 accounts for the mean of the absolute differences in the observed and predicted values. Lower
254 MAE is favourable.

255

256 **4. Results and Discussion**

257 **4.1 Streamflow simulation and evaluation of model performance**

258 The simulation (1979-2009) results generated under different rainfall scenarios (R_0 , R_1 , R_2
259 and R_3) on daily time scale for all five models (GLM, GAM, MARS, ANN and RF) is shown
260 in Table 3. R^2 values across models ranged from 0.71 to 0.90 and from 0.73 to 0.81 during
261 training and testing, respectively. Likewise, it was found that RSR and MAE varied from
262 0.55 to 0.31 and from 123.25 to 71.95 during training, as well as from 0.56 to 0.46 and
263 from 123.06 to 106.64 during testing, respectively. However, within models, RF performed
264 better at runoff prediction under all rainfall scenarios (R_0 , R_1 , R_2 , and R_3) compared to the
265 other models, while GLM showed the poorest results. R^2 , RSR and MAE values for the RF
266 model during the training ranged from 0.88 to 0.90, 0.32 to 0.34, 71.95 to 77.49, respectively.
267 Similar results were revealed during testing, with these falling between 0.76 and 0.78, 0.47
268 and 0.49, and 106.64 and 111.85, respectively. On the other hand, throughout training, the R^2 ,
269 RSR, and MAE values for the GLM model varied from 0.69 to 0.71, 0.54 to 0.55, and 134.80
270 to 140.56, respectively. During testing, they varied between 0.69 and 0.71, 0.54 and 0.56, and
271 134.35 and 141.26, respectively.

272 Table 3: Summary of model performance in simulating streamflow at Kasol

273

274 Figure 2, 3, 4 and 5 shows comparison of observed and simulated streamflow under rainfall
275 scenarios of R_0 , R_1 , R_2 and R_3 for all the models at Kasol, the outlet of the basin. As observed
276 from the Figures (2-5), RF was able to follow the curve better compared to the other models.



277 It is also deduced from the comparison of scatter plots wherein a relatively smaller deviation
278 in the observed and estimated discharge of streamflow was found for the RF model. GLM
279 performed the worst out of the five models with respect to the time variation graphs. A
280 limitation faced by all the five models was the simulation of peak values. The models slightly
281 underperformed at the prediction of higher values of streamflow. The model performed
282 slightly better during training than testing periods. Furthermore, it was observed that the
283 models with rainfall scenario R_3 had revealed reasonably better results in comparison to R_0 ,
284 R_1 and R_2 scenarios, indicating delayed contribution of rainfall-runoff to the river.

285 Figure 2: Comparison of observed and simulated streamflow for all five models (GLM,
286 GAM, MARS, ANN and RF) under rainfall scenarios R_0

287

288 Figure 3: Comparison of observed and simulated streamflow for all five models (GLM,
289 GAM, MARS, ANN and RF) under rainfall scenarios R_1

290

291 Figure 4: Comparison of observed and simulated streamflow for all five models (GLM,
292 GAM, MARS, ANN and RF) under rainfall scenarios R_2

293

294 Figure 5: Comparison of observed and simulated streamflow for all five models (GLM,
295 GAM, MARS, ANN and RF) under rainfall scenarios R_3

296

297 R^2 , RSR and MAE values across models under the rainfall scenario R_3 were found to range
298 from 0.71 to 0.90, 0.34 to 0.54, and 72 to 134.80 during training and from 0.71 to 0.90, 0.47
299 to 0.54, and 106.6 to 134.80 during testing. These findings led to the ultimate decision to use
300 the RF model with rainfall scenario R_3 to predict streamflow in the Sutlej River in the future
301 (2050s and 2080s) under the SSP245 and SSP585 scenarios.



302

303 **4.2 Annual streamflow changes in 2050s and 2080s under SSP245 and SSP585**

304 Figure 6 lists the projected change in mean annual streamflow for the Sutlej River in 2050s
305 and 2080s with respect to the base period (1979-2009) under different emission scenarios.
306 Out of six models, four (BCC-CSM2-MR, EC-Earth-3, INM-CM4.8, and INM-CM5.0)
307 projected an increase in annual streamflow in the 2050s and 2080s for both emission
308 scenarios. Depending on the model, it will be in the range of 0.46 to 2.84% in the 2050s and
309 from 1.32 to 4.37% in the 2080s under SSP245 scenario. The models with the lowest
310 increases in mean annual streamflow are BCC-CSM2-MR (0.46%) in the 2050s and INM-
311 CM4.8 (1.32%) in the 2080s, while INM-CM5.0 and EC-Earth-3 have shown the highest
312 increases (2.84% and 4.37%) in 2050s and 2080s, respectively. Similar to this, GCM models
313 predict that rise under SSP585 will vary between 0.18% (ACCESS- ESM1.5) and 3.16%
314 (EC-Earth-3) and 0.60% (ACCESS- ESM1.5) to 3.50% (EC-Earth-3) between 2050s and
315 2080s. However, a decrease in mean streamflow is predicted by ACCESS- ESM1.5 and
316 ACCESS- ESM2 in 2050s and 2080s under SSP245 and by ACCESS- ESM2 under SSP585.
317 It will range from -0.21 to -2.69% in 2050s and -0.35 to -2.21% in 2080s under SSP245 and
318 from -2.75 to -4.08% under SPP585. These variations in streamflow prediction from GCMs
319 may be attributed to their spatial resolution and parametrization levels (Singh et al., 2015c).
320 Therefore, in order to reduce uncertainty in projection of streamflow related to individual
321 GCMs, the yearly streamflow pattern of the Sutlej River was analysed also using the mean
322 ensemble of all six GCMs. According to the mean ensemble of the models, between 2050 and
323 2080, the Sutlej River's annual stream flow will increase by 5.51 to 6.04 percent for SSP585
324 and by 6.65 to 6.75 percent for SSP245. In general, the rise is expected to be higher in 2080s
325 as compared to 2050s under both the scenarios. This rise in mean annual streamflow is
326 impacted largely by the substantial increase in precipitation predicted over the basin during



327 2050s and 2080s. It is also established by previous research on the Himalayan catchments
328 which revealed that changes in the amount and direction of precipitation are significantly
329 more powerful predictors of water availability in the catchment than the presence of glaciers
330 (Miller et al., 2022).

331 Figure 6: Predicted change in mean annual streamflow of the Sutlej River with respect to the
332 reference period (1979-2009) in 2050s and 2080s under SSP245 and SSP585 for different
333 GCMs

334

335 Further, the projected streamflow patterns for the Sutlej River under SSP245 and SSP585 for
336 the 2050s and 2080s show similar tendencies, but with differing magnitudes, that have been
337 found by past researchers using process-based hydrological models. For instance, Singh et al.
338 (2015 a) used the SWAT (Soil Water Assessment Tool) model, a semi-distributed
339 hydrological model, to simulate streamflow for future periods using two CMIP3 models
340 (CGCM3 and HadCM3), and they discovered that the Sutlej River's mean annual streamflow
341 would increase in the range of 0.6 to 7.8% in the 2080s under higher emission scenario of A2,
342 which is equivalent to the SSP585 of the CMIP6. Similar to this, using the Variable
343 Infiltration Capacity (VIC) and SWAT models, respectively, Ali et al. (2018) and Shukla et
344 al. (2022) estimated increases in the Sutlej River's mean annual streamflow for the 2050s and
345 2080s under RCP4.5 and RCP8.5. The study of Shukla et al. (2022) estimates that under
346 RCP4.5 and RCP8.5, the mean streamflow of the river will increase by 14 and 21%,
347 respectively, in the 2080s. The relatively higher increase in the projected streamflow may be
348 attributed to the model's input variables (rainfall and temperature), which were derived from
349 CORDEX CCSM4 experiments, a regional climate model.

350

351 **4.3 Seasonal streamflow changes in 2050s and 2080s under SSP245 and SSP585**



352 The projected change in seasonal streamflow of the Sutlej River in 2050s and 2080s is shown
353 in the Figure 7. It is observed that all models for all scenarios indicated an increase in
354 streamflow during the post-monsoon and winter season in the 2050s and 2080s, while a
355 decrease in streamflow is seen in 2080s under higher GHG scenarios during the pre-
356 monsoon. Four out of six models predict rise in streamflow under both the scenarios in 2050s
357 (excluding under SSP245) and 2080s during monsoon season. Further, across the models and
358 within scenarios, there is a considerable difference in the seasonal streamflow predictions. It
359 will vary from +9.77% (BCC-CSM2-MR) to +15.56% (ACCESS- ESM2) in the 2050s and
360 from +10.77% (ACCESS- ESM1.5) to 18.28% (ACCESS- ESM2) in the 2080s during winter
361 season, from +5.17% (INM-CM5.0) to +39.86% (BCC-CSM2-MR) and from +1.85% (INM-
362 CM4.8) to +46.98% (BCC-CSM2-MR) during post-monsoon season, from -4.31% (EC-
363 Earth-3) to +7.49% (INM-CM5.0) and from -5.65% (EC-Earth-3) to +5.61% (INM-CM5.0)
364 during pre-monsoon seasons, and from -5.20% (ACCESS- ESM2) to +1.91% (INM-CM5.0)
365 and from -7.90% (ACCESS-ESM2) to +5.00% (INM-CM54.8) during monsoon season under
366 SSP245 scenario. Similarly, under scenario SSP585, it will vary from +9.80% (BCC-CSM2-
367 MR) to +15.15% (INM-CM5.0) in the 2050s and from +9.34% (BCC-CSM2-MR) to
368 +18.39% (INM-CM5.0) in the 2080s during winter season, from +1.30% (INM-CM5.0) to
369 +41.94% (BCC-CSM2-MR) and from +0.42% (ACCESS- ESM1.5) to +48.54% (BCC-
370 CSM2-MR) during post-monsoon season, from -7.28% (INM-CM4.8) to -0.11% (ACCESS-
371 ESM1.5) and from -10.03% (INM-CM4.8) to -2.22% (ACCESS- ESM1.5) during pre-
372 monsoon seasons, and from -7.95% (ACCESS- ESM2) to +6.78% (EC-Earth-3) and from -
373 6.29% (ACCESS- ESM2) to +8.15% (INM-CM4.8) during monsoon season. It is observed
374 that within seasons, maximum (+48.54%) and minimum (-10.03%) changes are predicted in
375 2080s under SSP585 during post-monsoon and pre-monsoon seasons, respectively.



376 Figure 7: Predicted change in seasonal streamflow pattern of the Sutlej River with respect to
377 the reference period (1979-2009) in 2050s and 2080s under SSP245 and SSP585 for different
378 GCMs

379

380 However, mean ensembles of models predicted a rise in streamflow of the Sutlej River in all
381 seasons in the 2050s and 2080s under both emission scenarios, with the exception of the pre-
382 monsoon, where streamflow is estimated to decrease in the 2080s under SSP585. In the
383 2050s, this will range from +5.60 to +5.99% the winter, +10.28 to +13.16% during the post-
384 monsoon, +2.02 to 6.66% during the pre-monsoon, and +8.75 to +10.63% during the
385 monsoon. In the 2080s, this will range from +6.30 to +6.47% percent during the winter,
386 +9.93 to +10.14% during the post-monsoon, -1.09 to +3.48% during the pre-monsoon, and
387 +11.07 to +11.43% during the monsoon.

388

389 **4.4. Monthly Streamflow Changes in 2050s and 2080s under SSP245 and SSP585**

390 Figure 8 illustrates how mean monthly streamflow patterns will alter in 2050s and 2080s
391 under both GHGs scenarios (SSP245 and SSP585) for different GCMs. A considerable
392 variation in the streamflow pattern is observed within months and for the models. All six
393 models generally in both scenarios expected an increase in monthly streamflow from January
394 to April and a reduction in June. It will range from +0.78 to +11.89% in January, from +5.07
395 to +18.17% in February, from +3.30 to +30.45% in March, from +13.20 to +50.52% in April,
396 and from -21.35 to -6.97% in June. However, no clear pattern is seen for the other months of
397 the year. For instance, three (BCC-CSM2-MR, EC-Earth-3 and INM-CM4.8) out of six
398 GCMs projected a reduction in streamflow for the months of May (-15.97 to -0.10%), while
399 four (ACCESS- ESM2.0, BCC-CSM2-MR, EC-Earth-3 and INM-CM4.8) predicted
400 reduction ranging between -16.35 to -0.75% for July under all scenarios. However, all GCMs



401 showed an increase in streamflow during the months of November (+0.94 to +29.75%) and
402 December (+0.10 to +7.81%), with the exception of INM-CM5.0 (in November) and
403 ACCESS-ESM1.5 (in December) that predicted decline in the streamflow ranging from -2.42
404 to -0.80% and to -1.08 to -0.14% for the same period.

405 Figure 8: Predicted change in monthly streamflow pattern of the Sutlej River with respect to
406 the reference period (1979-2009) in 2050s and 2080s under SSP245 and SSP585 for different
407 GCMs

408

409 The pattern of projected streamflow derived from the mean ensembles of the models, on the
410 other hand, is consistent for both the future periods under SSP245 and SSP585, and it
411 exhibits relatively less variability across the months (Figure 8). With the exception of June,
412 November and December, the increase in streamflow is anticipated for every month of the
413 year under both scenarios in 2050s and 2080s. The maximum increase (+27.01%) in monthly
414 streamflow is predicted in April in 2050s under SSP245 whereas minimum (-4.42%) in June
415 under SSP585 for the same period. The findings of the current research work, which showed
416 that the majority of models, including mean ensembles of the mean, reveal a decline in the
417 pattern of the streamflow under both scenarios for all of the periods, were validated by the
418 findings of Ali et al (2018) and Shukla et al (2022) studies' predictions of a decline in
419 streamflow during May and June (Figure 9). This implies that the RF model can be
420 successfully applied to streamflow simulation and modelling in the Himalayan environment
421 where data availability is a constraint.

422 Figure 9: Comparison of monthly observed (1979-2009) and projected discharge of the multi-
423 model ensembles for period 2050s and 2080s under SSP245 and SSP585 scenarios

424

425 **5. Conclusion**



426 Five machine learning models, GLM, GAM, MARS, ANN, and RF, were tested in this study
427 to simulate rainfall-runoff responses over the hilly Sutlej River Basin in order to determine
428 the best model for simulating streamflow response to future climate change in the 2050s and
429 2080s under SSP245 and SSP585 using CMIP6 data. In terms of runoff prediction, RF
430 outperformed the other models, as per the statistical evaluation criteria (R^2 , RSR, and MAE),
431 whereas GLM produced the worst results. The RF model's R^2 , RSR, and MAE values during
432 training varied from 0.88 to 0.90, 0.32 to 0.34, and 71.95 to 77.49, respectively. However,
433 during testing, it ranged between 0.76 and 0.78, 0.47 and 0.49, and 106.64 and 111.85,
434 respectively. The developed RF model was then used to simulate streamflow responses for
435 six GCMs (ACCESS- ESM1.5, ACCESS- ESM2, BCC-CSM2-MR, EC-Earth-3, INM-
436 CM4.8, and INM-CM5.0) and the mean ensembles of the models to investigate the
437 implications of future climate change on the Sutlej River pattern in the 2050s and 2080s
438 under SSP245 and SSP585 emission scenarios.

439

440 Within months, seasons, years, and for the models, a considerable fluctuation in the
441 streamflow pattern is seen. These variations in streamflow prediction may be illustrated by
442 the variations in spatial resolution and parametrization levels of GCMs, which led to a
443 noticeable fluctuation in the anticipated amounts of temperature and precipitation during the
444 study periods. Therefore, the monthly, seasonal, and annual streamflow patterns of the Sutlej
445 River were also studied using the mean ensemble of all six GCMs in order to reduce
446 uncertainty in streamflow projection due to individual GCMs. Both emission scenarios
447 predict an increase in the Sutlej River's mean annual streamflow (6.65-6.75% under SSP245
448 and 5.51-6.04% under SSP585) as well as its seasonal streamflow in the 2050s and 2080s,
449 with the exception of the pre-monsoon season. The post-monsoon season (10.28–13.16%) in
450 the 2050s and the monsoon season (11.07–11.43%) in the 2080s are anticipated to experience



451 the highest seasonal increases. Similar to this, the rise in streamflow is predicted for every
452 month of the year under both the 2050s and 2080s scenarios, with the exception of June,
453 November, and December. The largest increase in streamflow is observed for April in the
454 2050s under SSP245 while the least increase is predicted for June with SSP585 over the same
455 time period. Additionally, the projected changes in the mean annual and seasonal streamflow
456 of the river are consistent with earlier research done using process-based physical
457 hydrological models. Thus, the outcomes of the overall study indicate that the random forest
458 model is efficient for simulating streamflow in the Himalayan catchment, and that water
459 availability will rise as a result of an increase in catchment precipitation, which would
460 eventually lead to an increase in hydropower generation. The administrators of local water
461 resources and the government organizations in charge of maintaining reservoirs downriver
462 may find these details on streamflow patterns to be of great use.

463

464



465 **Code Availability:** The codes developed for this study is made available to the readers on
466 reasonable request.

467

468 **Data Availability:** The observed station data are confidential and authors do not have
469 permission for sharing the data.

470

471 **Author's Contribution**

472 DS and SL conceptualized the problems, supervised the entire research activity from its
473 inception to the completion, contributed in data collection, processing, interpretation and
474 wrote the research paper. MV and RS contributed in the development of model, generation of
475 figures and analysis of data. PC contributed in the data analysis and interpretation.

476

477 **Statements and Declarations**

478 The authors declare that they have no known competing financial interests or personal
479 relationships that could have appeared to influence the work reported in this paper.

480

481 **Acknowledgement**

482 Authors acknowledge National Natural Science Foundation of China (NFSC Grant no.
483 42171129) for funding this research work, and Bhakara Beas Management Board (BBM),
484 India for the hydro-meteorological data used in this study. We thank Ms. Pratibha
485 Shrivastava, a fourth-year B.Tech computer science student from NIT Raipur, for her help in
486 building the model.

487

488

489



490 **References**

- 491 Ali, S. A., Aadhar, S., Shah, H. L., & Mishra, V. (2018). Projected increase in hydropower
492 production in India under climate change. *Scientific Reports*, 8(1), 1-12.
- 493 Archer, D. (2003). Contrasting hydrological regimes in the upper Indus Basin. *Journal of*
494 *Hydrology*, 274(1-4), 198-210.
- 495 Beven, K. J. (2011). *Rainfall-runoff modelling: the primer*. John Wiley & Sons.
- 496 Conan, C., de Marsily, G., Bouraoui, F., & Bidoglio, G. (2003). A long-term hydrological
497 modelling of the Upper Guadiana river basin (Spain). *Physics and Chemistry of the*
498 *Earth, Parts A/B/C*, 28(4-5), 193-200.
- 499 Dai, A., Qian, T., Trenberth, K. E., & Milliman, J. D. (2009). Changes in continental
500 freshwater discharge from 1948 to 2004. *Journal of climate*, 22(10), 2773-2792.
- 501 Easterling, D. R., Meehl, G. A., Parmesan, C., Changnon, S. A., Karl, T. R., & Mearns, L. O.
502 (2000). Climate extremes: observations, modeling, and impacts. *Science*, 289(5487),
503 2068-2074.
- 504 Gao, Y., Gao, X., & Zhang, X. (2017). The 2 C global temperature target and the evolution of
505 the long-term goal of addressing climate change—from the United Nations
506 framework convention on climate change to the Paris agreement. *Engineering*, 3(2),
507 272-278.
- 508 Gerten, D., Rost, S., von Bloh, W., & Lucht, W. (2008). Causes of change in 20th century
509 global river discharge. *Geophysical Research Letters*, 35(20).
- 510 Goswami, B. N., Venugopal, V., Sengupta, D., Madhusoodanan, M. S., & Xavier, P. K.
511 (2006). Increasing trend of extreme rain events over India in a warming environment.
512 *Science*, 314(5804), 1442-1445.



- 513 Hastie, T., Tibshirani, R., Friedman, J. H., & Friedman, J. H. (2009). The elements of
514 statistical learning: data mining, inference, and prediction (Vol. 2, pp. 1-758). New
515 York: springer.
- 516 Herath, H. M. V. V., Chadalawada, J., & Babovic, V. (2021). Hydrologically informed
517 machine learning for rainfall–runoff modelling: towards distributed modelling.
518 *Hydrology and Earth System Sciences*, 25(8), 4373-4401.
- 519 Kabir, S., Patidar, S., & Pender, G. (2020, April). Investigating capabilities of machine
520 learning techniques in forecasting stream flow. In *Proceedings of the Institution of
521 Civil Engineers-Water Management* (Vol. 173, No. 2, pp. 69-86). Thomas Telford
522 Ltd.
- 523 Kirchner, J. W. (2006). Getting the right answers for the right reasons: Linking
524 measurements, analyses, and models to advance the science of hydrology. *Water
525 Resources Research*, 42(3).
- 526 Krysanova, V., Wortmann, M., Bolch, T., Merz, B., Duethmann, D., Walter, J., ... &
527 Kundzewicz, Z. W. (2015). Analysis of current trends in climate parameters, river
528 discharge and glaciers in the Aksu River basin (Central Asia). *Hydrological Sciences
529 Journal*, 60(4), 566-590.
- 530 Kundzewicz, Z. W., Nohara, D., Tong, J., Oki, T., Buda, S., & Takeuchi, K. (2009).
531 Discharge of large Asian rivers–Observations and projections. *Quaternary
532 International*, 208(1-2), 4-10.
- 533 Lutz, A. F., ter Maat, H. W., Wijngaard, R. R., Biemans, H., Syed, A., Shrestha, A. B., ... &
534 Immerzeel, W. W. (2019). South Asian river basins in a 1.5 C warmer world.
535 *Regional Environmental Change*, 19(3), 833-847.
- 536 Mahato, P. K., Singh, D., Bharati, B., Gagnon, A. S., Singh, B. B., & Brema, J. (2022).
537 Assessing the impacts of human interventions and climate change on fluvial flooding



- 538 using CMIP6 data and GIS-based hydrologic and hydraulic models. Geocarto
539 International, 1-26.
- 540 Masse-Dufresne, J., Barbecot, F., Baudron, P., & Gibson, J. (2021). Quantifying floodwater
541 impacts on a lake water budget via volume-dependent transient stable isotope mass
542 balance. *Hydrology and Earth System Sciences*, 25(6), 3731-3757.
- 543 Miller, J. D., Immerzeel, W. W., & Rees, G. (2012). Climate change impacts on glacier
544 hydrology and river discharge in the Hindu Kush–Himalayas. *Mountain Research and
545 Development*, 32(4), 461-467.
- 546 Mishra V, Bhatia U, Tiwari A.D. 2020. Bias-corrected climate projections for South Asia
547 from Coupled Model Intercomparison Project-6. *Sci. Data*. 7, 338.
548 <https://doi.org/10.1038/s41597-020-00681-1>.
- 549 Muhammad Adnan, R., Yuan, X., Kisi, O., Yuan, Y., Tayyab, M., & Lei, X. (2019, June).
550 Application of soft computing models in streamflow forecasting. In *Proceedings of
551 the institution of civil engineers-water management* (Vol. 172, No. 3, pp. 123-134).
552 Thomas Telford Ltd.
- 553 Nepal, S., & Shrestha, A. B. (2015). Impact of climate change on the hydrological regime of
554 the Indus, Ganges and Brahmaputra river basins: a review of the literature.
555 *International Journal of Water Resources Development*, 31(2), 201-218.
- 556 Otto, F. E., Skeie, R. B., Fuglestedt, J. S., Berntsen, T., & Allen, M. R. (2017). Assigning
557 historic responsibility for extreme weather events. *Nature Climate Change*, 7(11),
558 757-759.
- 559 Pasquini, A. I., & Depetris, P. J. (2007). Discharge trends and flow dynamics of South
560 American rivers draining the southern Atlantic seaboard: An overview. *Journal of
561 Hydrology*, 333(2-4), 385-399.



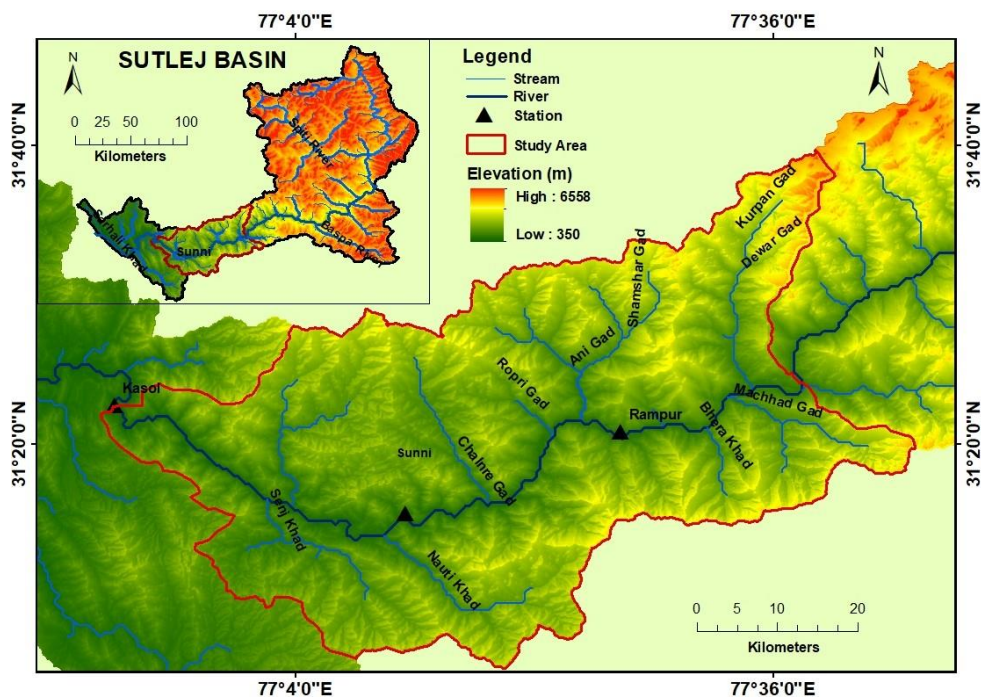
- 562 Riahi, K., Van Vuuren, D. P., Kriegler, E., Edmonds, J., O'Neill, B. C., Fujimori, S., ... &
563 Tavoni, M. (2017). The shared socioeconomic pathways and their energy, land use,
564 and greenhouse gas emissions implications: an overview. *Global Environmental*
565 *Change*, 42, 153-168.
- 566 Schreiner-McGraw, A. P., & Ajami, H. (2020). Impact of uncertainty in precipitation forcing
567 data sets on the hydrologic budget of an integrated hydrologic model in mountainous
568 terrain. *Water Resources Research*, 56(12), e2020WR027639.
- 569 Shortridge, J. E., Guikema, S. D., & Zaitchik, B. F. (2016). Machine learning methods for
570 empirical streamflow simulation: a comparison of model accuracy, interpretability,
571 and uncertainty in seasonal watersheds. *Hydrology and Earth System Sciences*, 20(7),
572 2611-2628.
- 573 Shukla, S., Jain, S. K., & Kansal, M. L. (2021). Hydrological modelling of a snow/glacier-fed
574 western Himalayan basin to simulate the current and future streamflows under
575 changing climate scenarios. *Science of The Total Environment*, 795, 148871.
- 576 Singh, D., Gupta, R. D., & Jain, S. K. (2014). Study of long-term trend in river discharge of
577 Sutlej River (NW Himalayan region). *Geography, Environment, Sustainability*, 7(3),
578 87-96.
- 579 Singh, D., Gupta, R. D., & Jain, S. K. (2015a). Assessment of impact of climate change on
580 water resources in a hilly river basin. *Arabian Journal of Geosciences*, 8(12), 10625-
581 10646.
- 582 Singh, D., Gupta, R. D., & Jain, S. K. (2015b). Statistical analysis of long term spatial and
583 temporal trends of temperature parameters over Sutlej river basin, India. *Journal of*
584 *Earth System Science*, 124(1), 17-35.



- 585 Singh, D., Jain, S. K., & Gupta, R. D. (2015c). Statistical downscaling and projection of
586 future temperature and precipitation change in middle catchment of Sutlej River
587 Basin, India. *Journal of Earth System Science*, 124(4), 843-860.
- 588 Singh, D., Rai, S. P., & Rai, D. (2019). Application of geospatial techniques in hydrological
589 modelling. In *Sustainable Green Technologies for Environmental Management* (pp.
590 167-173). Springer, Singapore.
- 591 Singh, P., & Jain, S. K. (2002). Snow and glacier melt in the Satluj River at Bhakra Dam in
592 the western Himalayan region. *Hydrological Sciences Journal*, 47(1), 93-106.
- 593 Singh, D., Zhu, Y., Liu, S., Srivastava, P. K., Dharpure, J. K., Chatterjee, D., ... & Gagnon,
594 A. S. (2022). Exploring the links between variations in snow cover area and climatic
595 variables in a Himalayan catchment using earth observations and CMIP6 climate
596 change scenarios. *Journal of Hydrology*, 608, 127648.
- 597 Sood, A., & Smakhtin, V. (2015). Global hydrological models: a review. *Hydrological
598 Sciences Journal*, 60(4), 549-565.
- 599 Stahl, K., Hisdal, H., Hannaford, J., Tallaksen, L. M., Van Lanen, H. A. J., Sauquet, E., ... &
600 Jódar, J. (2010). Streamflow trends in Europe: evidence from a dataset of near-natural
601 catchments. *Hydrology and Earth System Sciences*, 14(12), 2367-2382.
- 602 Stahl, K., Tallaksen, L. M., Hannaford, J., & Van Lanen, H. A. J. (2012). Filling the white
603 space on maps of European runoff trends: estimates from a multi-model ensemble.
604 *Hydrology and Earth System Sciences*, 16(7), 2035-2047.
- 605 Trenberth, K. E. (2011). Changes in precipitation with climate change. *Climate Research*,
606 47(1-2), 123-138.
- 607 Trenberth, K. E., Fasullo, J. T., & Shepherd, T. G. (2015). Attribution of climate extreme
608 events. *Nature Climate Change*, 5(8), 725-730.



- 609 Van der Wiel, K., Wanders, N., Selten, F. M., & Bierkens, M. F. P. (2019). Added value of
610 large ensemble simulations for assessing extreme river discharge in a 2 C warmer
611 world. *Geophysical Research Letters*, 46(4), 2093-2102.
- 612 Yang, Q., Zhang, H., Wang, G., Luo, S., Chen, D., Peng, W., & Shao, J. (2019). Dynamic
613 runoff simulation in a changing environment: A data stream approach. *Environmental*
614 *Modelling & Software*, 112, 157-165.
- 615 Lutz, A. F., Immerzeel, W. W., Shrestha, A. B., & Bierkens, M. F. P. (2014). Consistent
616 increase in High Asia's runoff due to increasing glacier melt and precipitation. *Nature*
617 *Climate Change*, 4(7), 587-592.
- 618 Zhu, Y., Liu, S., Yi, Y., Xie, F., Grünwald, R., Miao, W., ... & Singh, D. (2021). Overview of
619 terrestrial water storage changes over the Indus River Basin based on
620 GRACE/GRACE-FO solutions. *Science of The Total Environment*, 799, 149366.
- 621

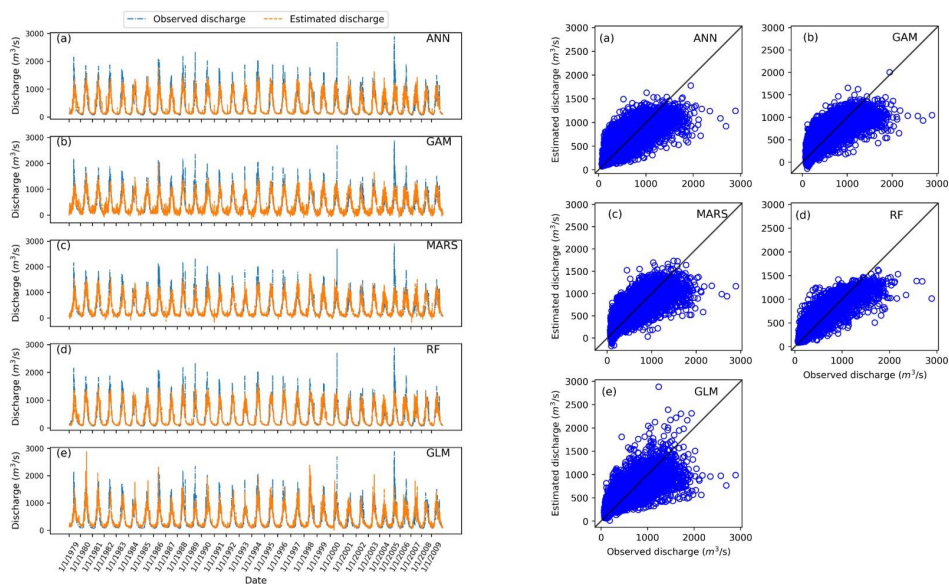


622

623

624

Figure 1: The location of the sub-catchment within Sutlej River Basin



625

626

Figure 2: Comparison of observed and simulated streamflow for all five models (GLM,

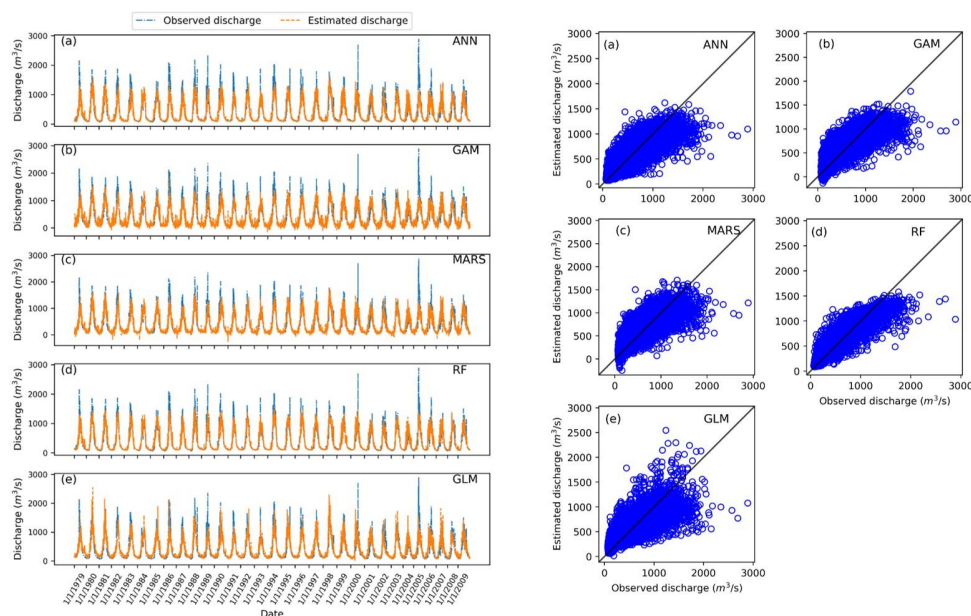
627

GAM, MARS, ANN and RF) under rainfall scenarios R_0

628



629

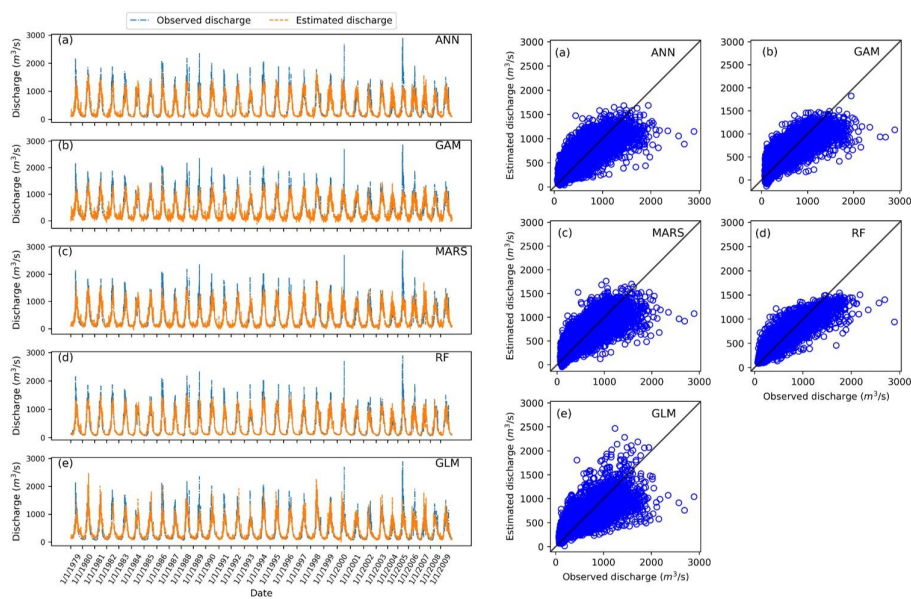


630

631 Figure 3: Comparison of observed and simulated streamflow for all five models (GLM,

632 GAM, MARS, ANN and RF) under rainfall scenarios R_1

633

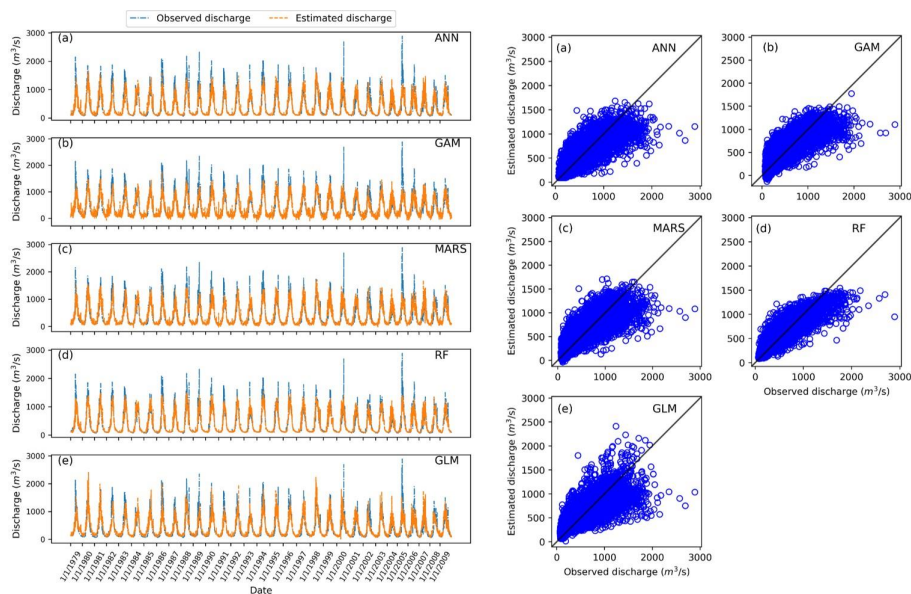


634

635 Figure 4: Comparison of observed and simulated streamflow for all five models (GLM,

636 GAM, MARS, ANN and RF) under rainfall scenarios R_2

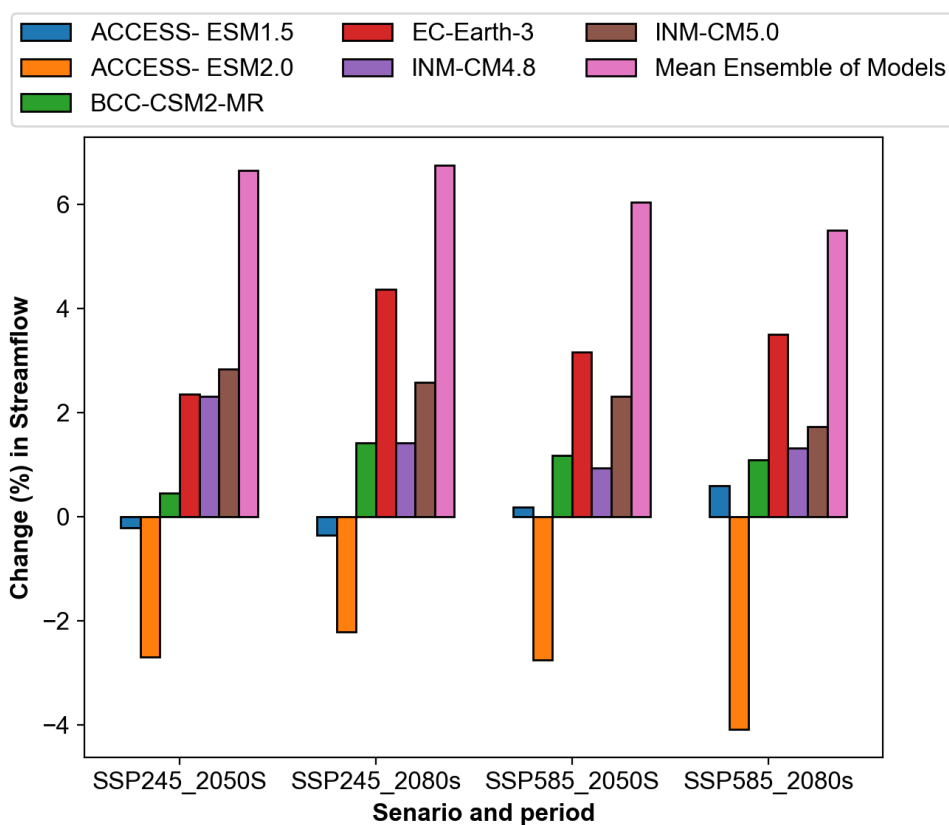
637



638

639 Figure 5: Comparison of observed and simulated streamflow for all five models (GLM,
640 GAM, MARS, ANN and RF) under rainfall scenarios R_3

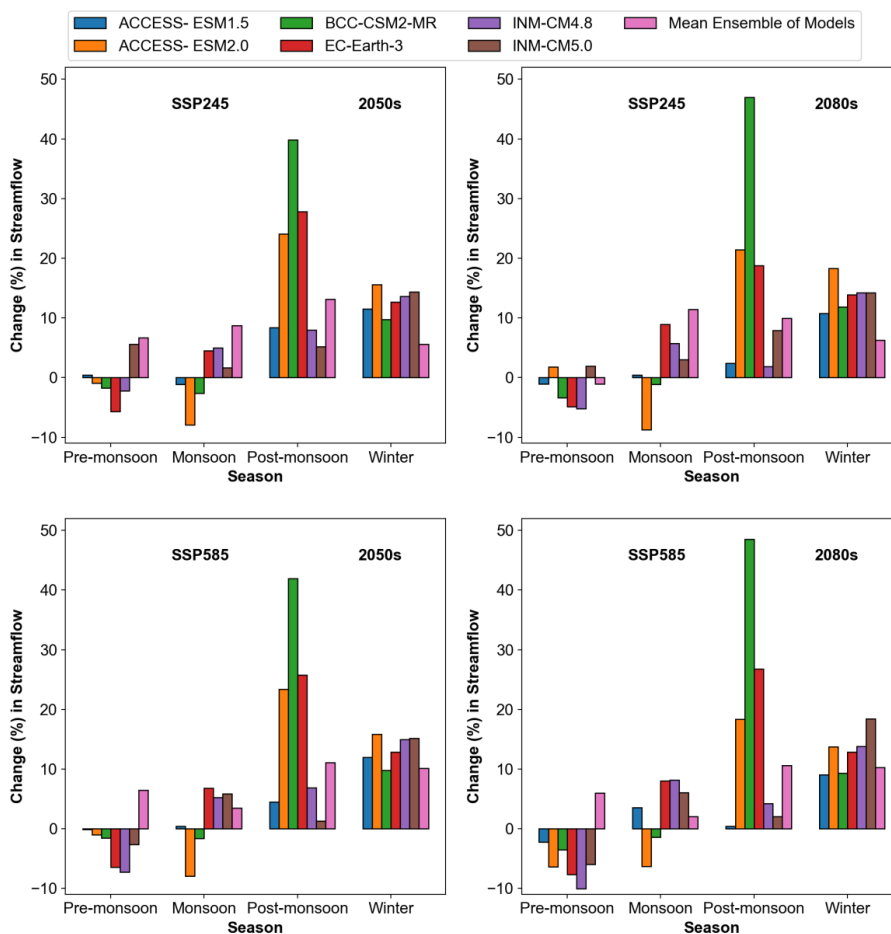
641



642

643 Figure 6: Predicted change in mean annual streamflow of the Sutlej River with respect to the
644 reference period (1979-2009) in 2050s and 2080s under SSP245 and SSP585 for different
645 GCMs

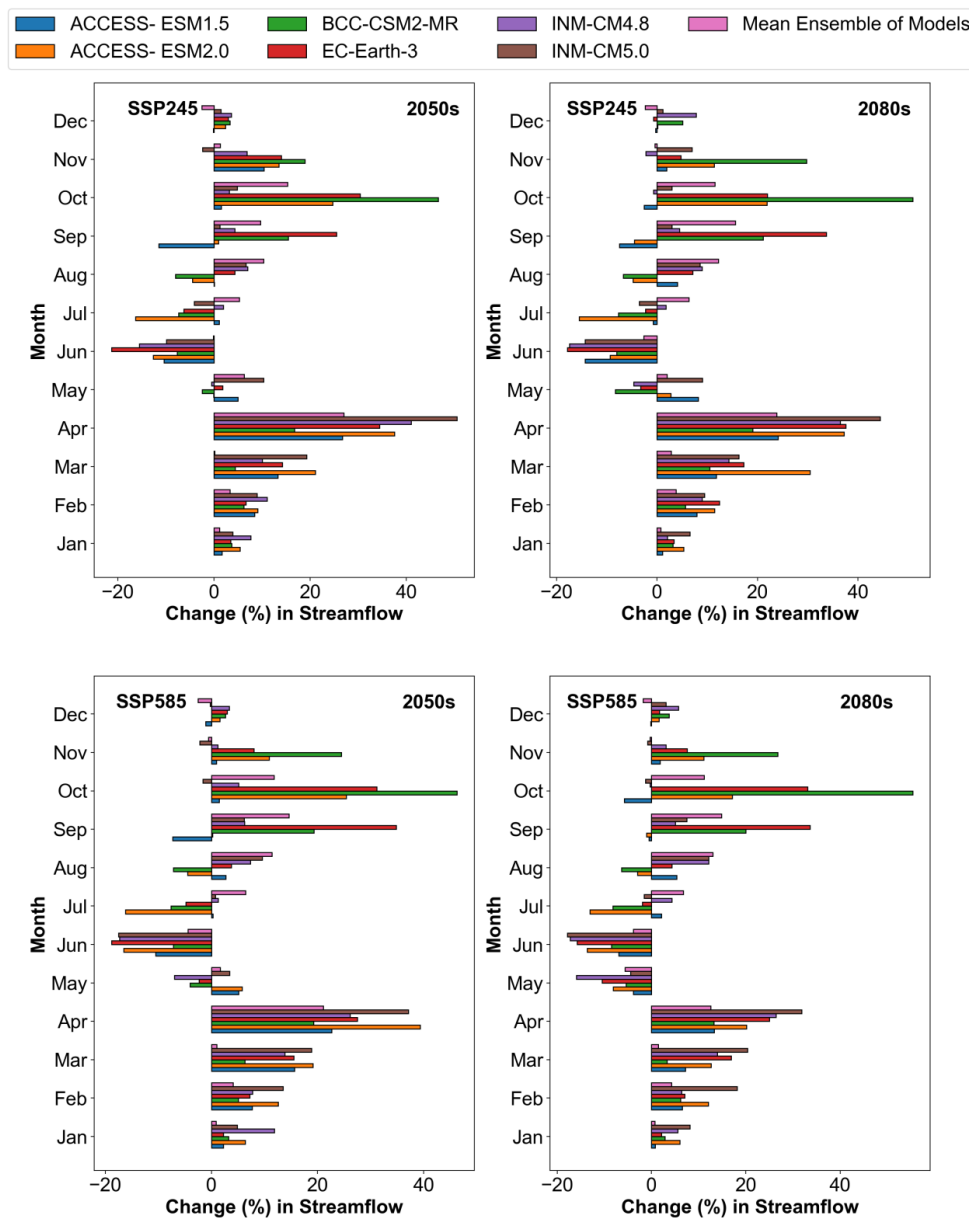
646



647

648 Figure 7: Predicted change in seasonal streamflow pattern of the Sutlej River with respect to
 649 the reference period (1979-2009) in 2050s and 2080s under SSP245 and SSP585 for different
 650 GCMs

651



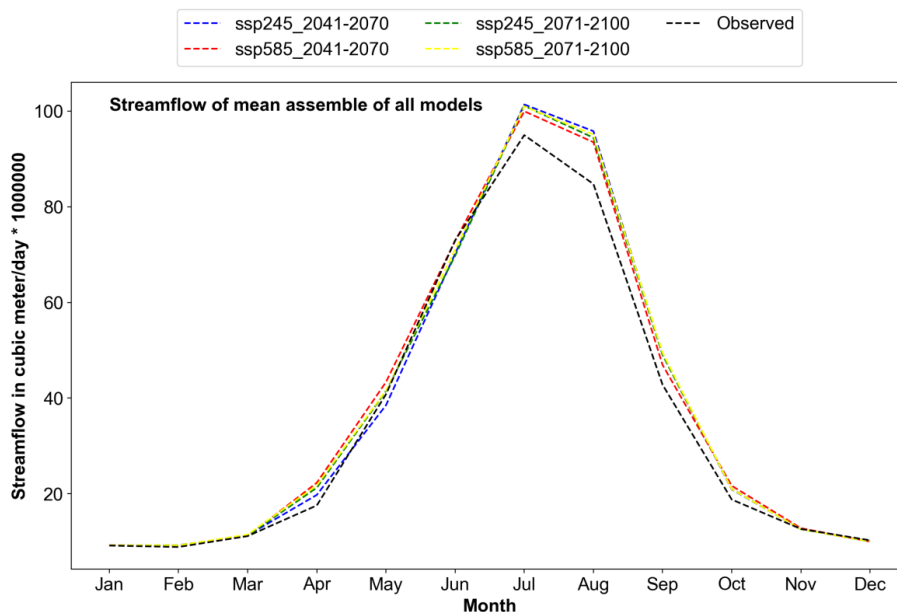
652

653 Figure 8: Predicted change in monthly streamflow pattern of the Sutlej River with respect to

654 the reference period (1979-2009) in 2050s and 2080s under SSP245 and SSP585 for different

655 GCMs

656



657

658 Figure 9: Comparison of monthly observed (1979-2009) and projected discharge of the multi-
659 model ensembles for period 2050s and 2080s under SSP245 and SSP585 scenarios

660



661

662 **Table 1:** Characteristics of the study catchment over the evaluation period of 1979–2009

Parameters	Details
Details of the sub-catchment	
Drainage area of the sub-catchment (km ²)	2457 km ²
Altitude	~500-5000 m
Slope	0-80°
Geology	Granite, Jutogh formation and Chail/Salkhala/Hemanta formation
Soil	Dystric cambisols, dystric regosols, and eutric fluvisols.
Streamflow measured at the outlet (Kasol) of the sub-catchment	
Average of annual streamflow	12469.43 m ³ /s
Minimum streamflow	64.30 m ³ /s
Maximum streamflow	2891.00 m ³ /s
Standard deviation (SD) of annual streamflow	1750.70 m ³ /s
Coefficient of variation (CV) of annual streamflow	0.14 m ³ /s
Rainfall integrated over the sub-catchment	
Average of annual rainfall	1001.32mm
Average of monsoon rainfall (July-September)	403.08mm
Average of winter rainfall (December-March)	277.35mm
Temperature integrated over the sub-catchment	
Average annual maximum temperature (T _{max})	28.35°C
Average annual minimum temperature (T _{min})	13.98°C

663

664



665 **Table 2:** The information on hyper parameters used for estimating model parameters

Model Name	Hyperparameter	Values
Random Forest (RF)	n_estimators, criterion, max_depth, min_samples_split, min_samples_leaf, min_weight_fraction_le af, max_features, max_leaf_nodes, min_impurity_decrease,	value=500 value="squared_error" value=None value = 2 value = 5 value = 0.0 value = auto value = None value = 0.0
Generalized Linear Model (GLM)	endog, exog, family, offset, exposure, freq_weights, var_weights, missing,	value = 1D value = 1D value = sm.families.Gaussian(sm .families.links.log()) value = None value = None value = None value = None value = str
Artificial Neural Network (ANN)	build_fn, warm_start, random_state, optimizer, loss, metrics, batch_size, validation_batch_size, verbose, callbacks, validation_split, shuffle, run_eagerly, epochs,	value = build_regressor value = False value = None value = rmsprop value = None value = None value = 64 value = None value = 1 value = None value = 0.0 value = True value = False value = 500
Multivariate Adaptive Regression Splines (MARS)	max_terms, max_degree , allow_missing, penalty, endspan_alpha, endspan, minspan_alpha, minspan, thresh , zero_tol, min_search_points, check_every, allow_linear,	value = 20 value = 3 value = False value = 3.0 value = 0.005 value = -1 value = 0.005 value = -1 value = 0.001 value = 1e-12 value = 100 value = -1 value = True



	use_fast, fast_K, fast_h, smooth, enable_pruning, feature_importance_type, feature_importance_type,	value = False value = 5 value = 1 value = False value = True value = None value = 0
Generalized Additive Model (GAM)	formula, family, data, weights, subset , na.action,offset, method, optimizer, control, scale, select, knots, sp, min.sp, H, gamma, fit, paraPen, G, drop.unused.levels, drop.intercept, discrete,	value = None value = gaussian() value = list() value = Null value = Null value = Null value = "GCV.Cp" value = c("outer","newton") value = list(), value = 0 value = False value = Null value = Null value = Null value = Null, value = 1 value = True value = Null value = Null value = True value = Null value = False

666

667



668

Table 3: Summary of model performance in simulating streamflow at Kasol

Model	Model inputs	Training			Testing		
		R ²	RSR	MAE	R ²	RSR	MAE
RF	R ₀ (rainfall on the same day), T _{max} , T _{min} , relative humidity, solar radiation and wind speed	0.88	0.34	77.5	0.76	0.49	111.9
	R ₁ (rainfall lagged by one day), T _{max} , T _{min} , relative humidity, solar radiation and wind speed	0.89	0.33	74.4	0.77	0.48	109.2
	R ₂ (rainfall lagged by two day), T _{max} , T _{min} , relative humidity, solar radiation and wind speed	0.90	0.32	73.1	0.78	0.47	107.5
	R ₃ (rainfall lagged by three day), T _{max} , T _{min} , relative humidity, solar radiation and wind speed	0.90	0.32	72.0	0.78	0.47	106.6
GLM	R ₀ (rainfall on the same day), T _{max} , T _{min} , relative humidity, solar radiation and wind speed	0.69	0.55	140.6	0.69	0.56	141.3
	R ₁ (rainfall lagged by one day), T _{max} , T _{min} , relative humidity, solar radiation and wind speed	0.70	0.54	137.3	0.70	0.55	137.5
	R ₂ (rainfall lagged by two day), T _{max} , T _{min} , relative humidity, solar radiation and wind speed	0.71	0.54	136.0	0.71	0.54	135.4
	R ₃ (rainfall lagged by three day), T _{max} , T _{min} , relative humidity, solar radiation and wind speed	0.71	0.54	134.8	0.71	0.54	134.5
ANN	R ₀ (rainfall on the same day), T _{max} , T _{min} , relative humidity, solar radiation and wind speed	0.73	0.52	123.3	0.73	0.52	123.0
	R ₁ (rainfall lagged by one day), T _{max} , T _{min} , relative humidity, solar radiation and wind speed	0.74	0.51	119.3	0.74	0.51	118.9
	R ₂ (rainfall lagged by two day), T _{max} , T _{min} , relative humidity, solar radiation and wind speed	0.75	0.50	119.3	0.75	0.50	118.2
	R ₃ (rainfall lagged by three day), T _{max} , T _{min} , relative humidity, solar radiation and	0.75	0.50	117.7	0.75	0.50	117.4



	wind speed						
MARS	R ₀ (rainfall on the same day), T _{max} , T _{min} , relative humidity, solar radiation and wind speed	0.77	0.48	118.9	0.79	0.45	112.8
	R ₁ (rainfall lagged by one day), T _{max} , T _{min} , relative humidity, solar radiation and wind speed	0.75	0.50	126.1	0.74	0.51	126.7
	R ₂ (rainfall lagged by two day), T _{max} , T _{min} , relative humidity, solar radiation and wind speed	0.75	0.50	124.8	0.75	0.50	125.0
	R ₃ (rainfall lagged by three day), T _{max} , T _{min} , relative humidity, solar radiation and wind speed	0.75	0.50	125.1	0.75	0.50	125.5
GAM	R ₀ (rainfall on the same day), T _{max} , T _{min} , relative humidity, solar radiation and wind speed	0.72	0.53	139.0	0.72	0.53	139.4
	R ₁ (rainfall lagged by one day), T _{max} , T _{min} , relative humidity, solar radiation and wind speed	0.74	0.51	136.2	0.73	0.52	136.9
	R ₂ (rainfall lagged by two day), T _{max} , T _{min} , relative humidity, solar radiation and wind speed	0.74	0.51	134.7	0.74	0.51	135.2
	R ₃ (rainfall lagged by three day), T _{max} , T _{min} , relative humidity, solar radiation and wind speed	0.74	0.50	133.8	0.74	0.51	134.8

669

670

671

672

673

674

675

676

677